Evidence for multiple Plio-Pleistocene lake episodes in the hyperarid Atacama Desert

Benedikt Ritter[a*], Steven A. Binnie[a] Finlay M. Stuart[b], Volker Wennrich[a], Tibor J. Dunai[a]

[a] Institute of Geology & Mineralogy, Zuelpicher Strasse 49b, 50674 Cologne - Germany University of Cologne, Germany

[b] Isotope Geosciences Unit, Scottish Universities Environmental Research Centre, East Kilbride G75 0QF, UK

Corresponding Author:

Benedikt Ritter – benedikt.ritter@uni-koeln.de

Suelzburgstrasse 122, D-50937 Cologne Germany

Keywords: cosmogenic nuclide exposure dating, Atacama Desert, lake shorelines

Abstract:

Cosmogenic nuclide exposure dating of ancient shoreline terraces of the Quillagua-Llamara Soledad Lake in the central Atacama Desert of northern Chile provides new insights in the paleohydrology of the driest desert on Earth. The lake developed in a paleo-endorheic drainage system in the Central Depression prior to draining into the Pacific due to incision of the Río Loa canyon. The durations of lake stages were sufficiently long to form wave-erosion induced shoreline terraces on the wind-exposed slopes of former islands. Successively younger shoreline levels are preserved over an elevation range of 250 m due to progressive uplift of the islands coeval with the lake stages. Cosmogenic ^{10}Be- and ^{21}Ne-derived exposure ages of the shorelines reveals that the hyperarid conditions in the Rio Loa catchment were interspersed by several pluvial stages during the Pliocene and Pleistocene, which generated a large and persistent lake in the Quillagua-Llamara basin. The exposure ages of the final lake stage provide the maximum age for the incision of the Río Loa canyon (274±74 ka) and the subsequent breaching of the Coastal Cordillera.

1. Introduction

The Atacama Desert of northern Chile is one of the driest places on Earth; the extreme hyperarid core (Coastal Cordillera, Central Depression; Fig. 1) receives less than 10 mm/yr of precipitation (Houston and Hartley, 2003). While the main factors controlling hyper-aridity in the Atacama Desert are established, the onset and permanence of hyper-aridity remain a matter of debate (e.g., Sillitoe and McKee, 1996; 1999; Hartley and Chong, 2002; Rech et al., 2003; Dunai et al., 2005; Nishiizumi et al., 2005; Latorre et al., 2006; Rech et al., 2006; Kober et al., 2007; Nester et al., 2007; Evenstar et al., 2009; Placzek et al., 2010; Gayo et al., 2012; Sáez et al., 2012; Jordan et al., 2014; Evenstar et al., 2017). The nearly stable position of the South American continent over the last 150 million years (Hartley et al., 2005) and the establishment of the Peru-Chile Current system at around 50 Ma (Cristini et al., 2012) support the notion that predominantly arid conditions persisted since the early Miocene (Dunai et al., 2005), and potentially even earlier (Hartley et al., 2005). Secular variations of the global climate system during the Cenozoic (Zachos et al., 2001) led to punctuations of the prevailing hyper-arid climate in the Atacama Desert by wetter (though still arid) periods (e.g., Betancourt et al., 2000; Dunai et al., 2005; Nester et al., 2007; 2009; Rech et al., 2010; Sáez et al., 2012; Jordan et al., 2014; Evenstar et al., 2017). These pluvial phases are evident from Miocene-Pliocene lacustrine and fluvial sediments in the Central Depression (e.g. Gaupp et al., 1999; Sáez et al., 2012; Kirk-Lawlor et al., 2013).

Here we present new insights into the timing of relatively wet periods in the Central Depression based on exposure dating of former shoreline terraces of the Quillagua-Llamara-Soledad lake. These terraces are preserved by uplift of topographic highs in the Quillagua-Llamara basin (QLB). New cosmogenic ^{10}Be and ^{21}Ne data constrain the timing of the most recent lacustrine phases, and the eventual draining of the Quillagua-Llamara-Soledad Lake by the incision of the Río Loa canyon.

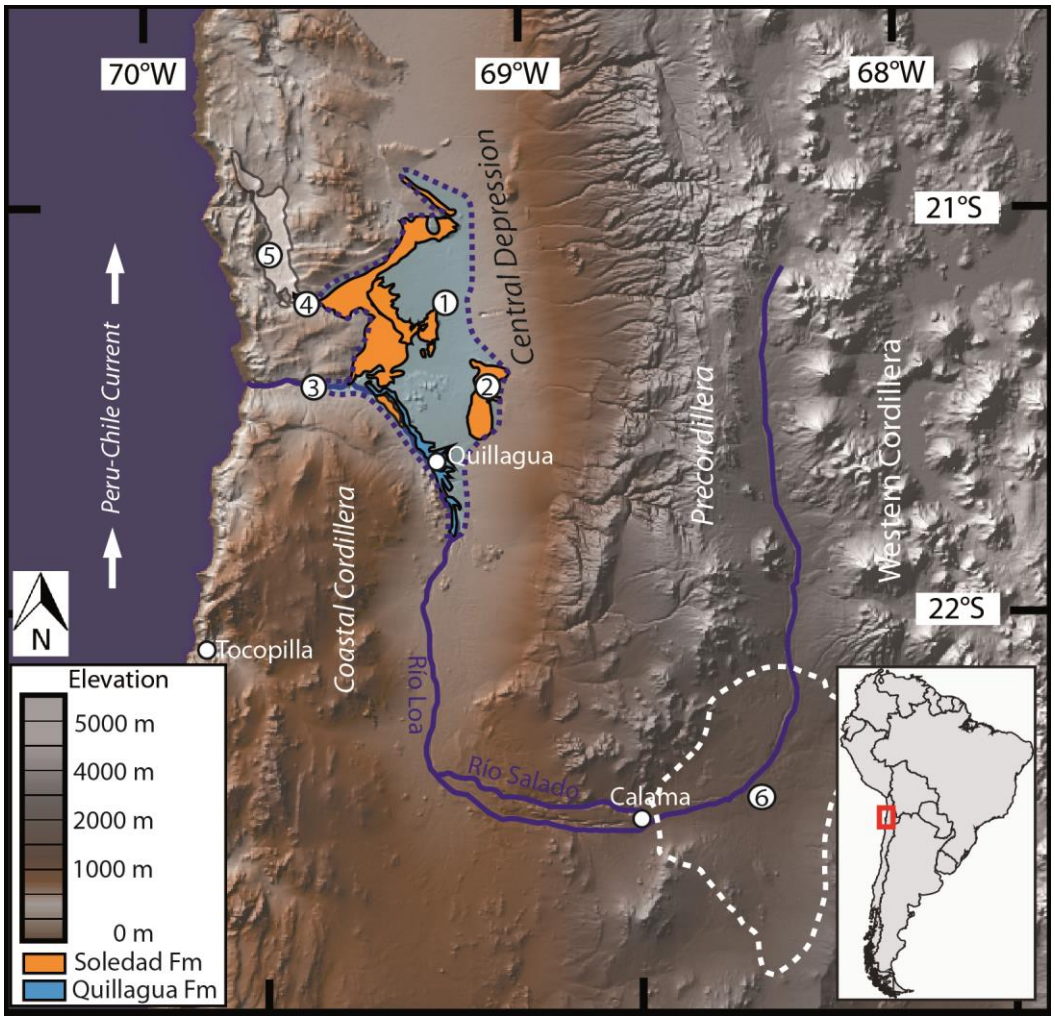

Fig. 1: Geographic setting of Quillagua-Llamara basin in the Central Depression (DEM based on ASTER GDEM data). Orange indicates outcrops of the Soledad Formation (Brüggen, 1950; 2012; Quezada et al., 2013). Blue indicates outcrops of the Quillagua Formation (Sáez et al., 2012). (1) Cerro Soledad, (2) Lomas de Sal, (3) Westernmost extension of former lake, overflow of Río Loa, (4) Montón de Gloria Pass (831m), (5) white area indicates Salar Grande, (6) dashed white line denotes the Calama basin. Translucent blue area indicates potential lake extension. *(Colour – Size: one-and-a-half-page width 140mm)*

2. Background

2.1 Regional Geology

The central Atacama Desert is located in the fore-arc region of the Central Andes in northern Chile (Fig. 1). The area includes three morphotectonic units; the Coastal Cordillera, Central Depression, and Precordillera. The latter is bordered by the Western Cordillera, forming an active volcanic arc (Fig. 1). The study area is located in the southern Central Depression, bound to the west by the Coastal Cordillera and to the east by the Precordillera. The Central Depression is a N-S elongated topographic basin that contains the Pampa de Tamarugal (PDT) and includes the QLB in the south (Fig. 1 translucent blue area). The Coastal Cordillera acts as a topographic barrier, prohibiting any appreciable sediment transport from the Precordillera to the Pacific Ocean. This has enabled the exceptional preservation of many tectonic deformation features that are caused by the coupling between the subducting oceanic Nazca plate and the South American plate in the Coastal Cordillera. E-W tectonic deformation commenced at least 6 million years ago, with fault slip rates that are typically less than 0.5 mm/year (Allmendinger and Gonzalez, 2010).

The incision of the Río Loa canyon transformed the QLB from an endorheic into an exorheic basin, while parts of the northern PDT, north of Quebrada Guatacondo, remained endorheic. Based on the age of the Soledad Formation this could have occurred during the late Pleistocene (Sáez et al., 2012) or early Pliocene (Quezada et al., 2013). Relict deposits of the former lacustrine and evaporitic facies and/or corresponding diagenetic equivalents of the Quillagua-Llamara-Soledad Lake (QLSL) are regionally widespread in the southern PDT (Fig. 1). These may reflect pluvial periods in the last 10 million years (Sáez et al., 2012). Although the sediment sequences have been dated several times, some ages are contradictory and allow alternative environmental reconstructions (Sáez et al., 1999; Sáez et al., 2012; Quezada et al., 2013; Jordan et al., 2014).

The Central Depression is a forearc basin (Jordan et al., 2014; Evenstar et al., 2017), bound to the west by normal faults in the Coastal Cordillera. The basement of the Central Depression consists of Palaeozoic and Mesozoic rocks, which are locally uplifted above the present-day valley floor. In

the study area, the depression is filled by up to 1000 m of Eocene to Pliocene alluvial and lacustrine sediments, interbedded with volcanoclastic deposits (Jensen et al., 1995; Sáez et al., 1999; Hartley and Evenstar, 2010; Jordan et al., 2010; Jordan et al., 2014). Alluvial fan deposits are derived almost exclusively from the Precordillera to the east (Carrizo et al., 2008; Nester, 2008; Jordan et al., 2014). The Tertiary PDT basin was formed by the combination of N-S and NW-SE orientated fault system activity, predominantly of currently supratenuous faults (Sáez et al., 1999). Neogene reverse faulting on the Precordillera fault zone has been confirmed for the northern PDT (Victor et al., 2004; Nester, 2008), as well for the southern part (Nester, 2008; Nester and Jordan, 2012). Studies indicate that fault systems in the Coastal Cordillera were reactivated during the past 6 Ma and their effects extend into the Central Depression (Allmendinger et al., 2005).

North to South trending elongated hills on Mesozoic basement in the PDT (Cerro Soledad Fig. 1, 3, Cerro Challacollo, and Cerro Longacho, see Nester (2008)) protrude up to 300 m above the plain. Carrizo et al. (2008) identified low angle reverse faults near the Salar de Bellavista to be responsible for the uplift of topographic highs after 18-19 Ma (see Fig. 16a in Carrizo et al., 2008). Evidence for young deformation within the basin can be found at Lomas de Sal (Fig. 1) where, a ~100 m thick Plio-Pleistocene sequence has been uplifted by reverse faulting (Nester, 2008). Geomorphological evidence for tectonic deformation in the vicinity includes folded diatomites at the base of Cerro Mogote (Sáez et al., 1999; for location see Fig. 3).

The detailed kinematics of the inferred uplift and deformation around Cerro Soledad, Cerro Mogote and Cerros de Hilaricos is poorly known. Recent mapping by SERNAGEOMIN (Quezada et al., 2012) provide a large scale framework for the structural geology, but the resolution of this mapping is not fine enough to resolve the tectonic kinematics around those exceptional highs within the Central Depression. Statements about the precise occurrence of faults and their appearance in conjunction with folds remain approximations and require more detailed studies.

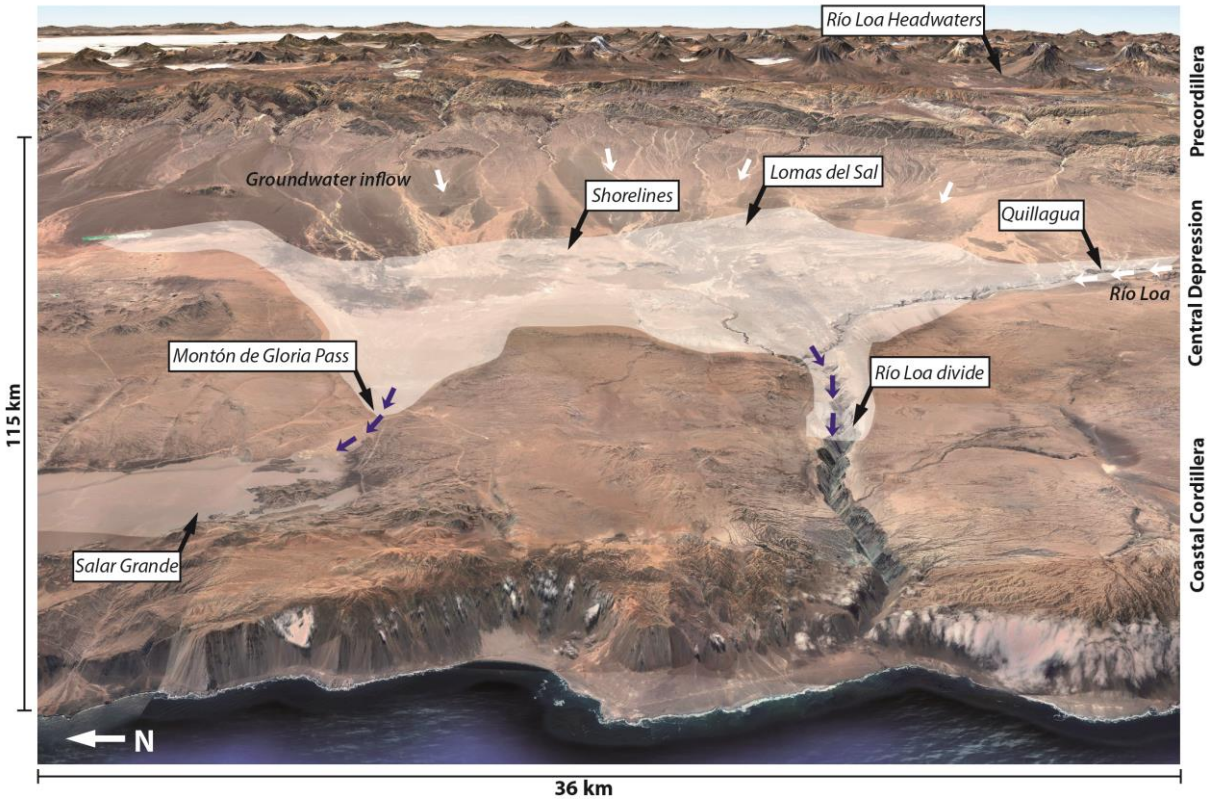

Fig. 2: Google Earth Satellite 3D Model (based on Image Landsat / Copernicus – Data SIO, NOAA, U.S. Navy, NGA, GEBCO) with a twofold altitude exaggeration. The pale shaded area displays potential lake extension based on outcrops. White arrows indicate major water inflow pathways, blue arrows mark overflow paths toward the (1) Salar Grande (present altitude 831m±10m) and (2) Río Loa (present altitude 830±10m). The latter was the outflow during the breach of the endorheic drainage system of the Quillagua basin. *(Colour – Size: Full Page width 190mm)*

2.2 Local Hydrology – Precipitation Pathways

The catchment of the QLB/Río Loa (32,820 km^2 from Houston, 2006c; Jordan et al., 2015a) derives the majority of its water from the Western Cordillera to the East. It drains into the QLB via groundwater flow and surface flow in the perennial Río Loa (Fig. 1, 2). Runoff and groundwater flow was higher during pluvial periods in the Plio-Pleistocene (Houston, 2006b).

Due to the temperature inversion above the cold Peru-Chile Current, westerly precipitation in the Atacama Desert originating from the Pacific Ocean is sparse. However, during infrequent rain events, surface drainage can occur due to precipitation coming from the Pacific as north migrating

low pressure systems are diverted (e.g. Bozkurt et al., 2016). Such sporadic westerly precipitation events include the flood of March 2015 in northern Chile, which brought significant precipitation, though this decreased with increasing altitude and was limited to south of Quillagua (Bozkurt et al., 2016; Wilcox et al., 2016). Such events are connected to the establishment of El Niño conditions favouring either cut-off north-migrating low-pressure cells from the Southern Westerlies (Vuille and Ammann, 1997), or destabilization and reduction of the temperature inversion at the Chilean coast (McKay et al., 2003). Climate models predict regional warming of the subtropical southeast Pacific during 'El Niño' conditions that effectively increase precipitation and moisture along the west coast of South America, and on the arid western slopes of the Andes due to the reduction of thermal subsidence and anticyclonic flow (Garreaud et al., 2010). Torrential rain during the 'El Niño' of 1997-98, for example, created the second largest lake in Peru in the Sechura Desert (Woodman, 1998). Earlier, long-lasting lake stages in the QLB are evidenced by lacustrine deposits of the Quillagua Formation, which suggest permanent 'El Niño-like' conditions persisted during the Pliocene (Sáez et al., 2012). Similar 'El Niño-like' conditions in the Atacama were also postulated for several wet periods during the Pleistocene (Ortlieb et al., 1996; Contreras et al., 2010; Wang et al., 2015). The main and more regular source of moisture is Atlantic air masses, despite depletion by orogenic rainfall at the eastern flanks of the Andes and in parts of the Altiplano. These easterly rains, which are enhanced during typical 'La Niña' conditions, are usually characterized by cooler atmospheric temperatures, easterly wind anomalies, and above average precipitation in the sub- to tropical western South America (Aceituno, 1988; Vuille, 1999; Vuille et al., 2000). The amplitude of 'La Niña' conditions in South America is governed by the strength and position of the Bolivian High (Vuille et al., 2000). A southward displacement and intensification of the Bolivian High hampers upper tropospheric westerly wind flow as well as strengthening easterlies and the corresponding moisture flux from the Amazon basin. These air masses spill over the Central Andes and reach the upper Western Andean flank (Vuille and Keimig, 2004) causing precipitation that decreases rapidly with elevation (Houston and Hartley, 2003). For instance, the source region of the Río Loa at around 4000 m receives about 100 mm rain per year, whereas the Río Loa valley in the Central Depression, at about 1000 m elevation (e.g. at

Quillagua Fig. 1, 2), has annual rainfall of less than 1 mm (Houston and Hartley, 2003). As aridity is controlled by large-scale atmospheric circulation patterns, the current orographic precipitation gradient pattern has most-likely persisted over the longer-term, despite the overall amounts of precipitation having varied (Jordan et al., 2014).

Presently the flow rates of the perennial Río Loa are 0.6 m^3/s (post 1976). In 1918 prior to the significant water extraction the discharge was 3.6 m^3/s (both measured at the outflow into the Pacific; Salazar, 2003). Due to the high annual evaporation rates (i.e. > 3500 mm/a at 1000 m elevation; Houston, 2006a) even the higher discharge rate could not sustain an expansive lake in the central valley. For example, the outcrops of the Soledad Formation indicated a minimum lake extension of ~2,570 km^3 requiring more than the recent perennial inflow of the Rìo Loa ($1.14*10^8$ m^3/a) to sustain a lake by high evaporation rate of $9.01*10^{13}$ m^3/a.

2.3 Lacustrine sediments of QLB

The sedimentary sequence of the QLB consists of alluvial strata, interbedded with lacustrine sequences and volcanoclastic deposits (Sáez et al., 1999, 2012). Fluvial sedimentation predominantly occurred to the south of Quillagua and was presumably controlled by the sediment input of the Proto-Río Loa, whereas lacustrine sedimentation was concentrated in the central basin around Cerro Mogote, Cerro Soledad, and Quillagua (Sáez et al., 2012) (Fig. 1, 2, 3a).

The first Miocene sediment units are gypsum-anhydrite cemented siliciclastic deposits of the Hilaricos Fm. These are overlain by diatomites, marls, silty limestones, gravelly sandstones, and occasional volcanoclastic deposits of the Quillagua Fm (Sáez et al., 1999). The final lacustrine episode of the QLSL is represented by the Soledad Fm, consisting of halite-gypsum evaporitic sediments with minor siliciclastics (Chong et al., 1999; Pueyo et al., 2001; Sáez et al., 2012, Fig. 1). Massive (>10 m thickness) open water evaporites with large, dm-scale, bottom nucleated chevron gypsum crystals, occur as erosive remnants along the eastern section of the southern margin of the Rio Loa canyon (this study, supplementary data).

193 The near-continuity of surficial deposits and the geochemical signature of the Soledad Fm
194 evaporites (Br-content and S-isotopes , Pueyo et al., 2001), support the notion of a temporary
195 connection between the QLB and the Salar Grande basin (Fig. 1, 2, Chong et al., 1999; Sáez et al.,
196 1999). This connection via the Montón de Gloria Pass (current elevation 830 m, Chong et al., 1999)
197 is thought to have been disrupted by fault reactivation in the Coastal Cordillera (Allmendinger et
198 al., 2005).

199 Outcrops of the Soledad Fm remnants (Quezada et al., 2012; Quezada et al., 2013) indicate a
200 minimum lake surface area of ~2,570 km^2 (Fig. 1, 6, this study). Spilling points at the Montón de
201 Gloria pass towards the Salar Grande (current elevation 831±10m, Chong et al., 1999; Pueyo et al.,
202 2001) and at the Río Loa (mean current elevation 830±10m, top of outcropping sediments, orange
203 surface in Fig. 1, westernmost reconstructed lake extension, Sáez et al., 1999), indicate the lake
204 level could not exceed 830 ± 10 m (Fig. 1, 2, 6). A higher lake level would have drained the basin,
205 presumably initiating the incision of the Río Loa. The elevation of present day outcrops of Soledad
206 Formation rocks may exceed the present day elevation of the spilling points (up to 220 m, Fig. 3)
207 due to differential tectonic uplift since deposition.

208 Although different approaches have been used to date the Soledad Fm, its chronology is still under
209 debate (Sáez et al., 2012; Quezada et al., 2013). Ar/Ar ages of tephra layers in the halite sequence
210 of the Lomas del Sal were used to constrain the deposition age of the lower Soledad formation to
211 between 0.21 ± 0.06 Ma and 0.098 ± 0.042 Ma (Sáez et al., 2012). However, four ash layers,
212 intercalated with anhydrite-sand successions of the Soledad Fm, exposed at Cerro Soledad, Salar
213 Sur Viejo and at Cerro Cachango, yield Ar/Ar ages between 3.16 ± 0.07 Ma and 3.73 ± 0.02Ma
214 Quezada et al. (2013). These contradictory ages mean that there is a considerable uncertainty in
215 both the spatial assignment of sediments to the Soledad formation and its deposition age.

216 2.4 Shoreline terraces

217 The conspicuous linear features at Cerro Soledad were first suggested by Brüggen (1950) to
218 represent abandoned shorelines (Fig. 3) of a lake, which was around 80 m deep. Subsequent

studies suggested that the lake was deeper (200 m, Hollingworth, 1964). Stoertz and Ericksen (1974) and Naranjo and Paskoff (1982) noted that the former shorelines are not level, reflecting differential tectonic uplift across the region. In an alternative hypothesis, Rieu (1975) interpreted these linear features as a result of uplift and tectonic displacement in a horst-graben structure, without invoking the presence of a lake. Naranjo and Paskoff (1982) identified four distinct shoreline levels at Cerro Soledad, spanning more than 200 m vertical distance, and reported abundant well-rounded pebbles on all levels. They assigned the rounding of these pebbles to wave action of the paleo-lake 'gran lago salado de Soledad (*sensu* Brüggen, 1950)'. These shorelines are mostly cut into halite (Naranjo and Paskoff, 1982) but also into underlying bedrock (this work; see also Fig. 3). The occurrence of pebbles is laterally limited to bedrock outcrops and pebbles are of the same lithology as the underlying bedrock (this study). Presently all but the lowest shorelines are above the current elevation of topographic spilling points of the paleo-lake (Fig. 2), indicating significant differential tectonic movement since the creation of the shorelines.

The hypothesis that an ephemeral lake was responsible for the creation of the linear features on the Cerro Soledad and neighbouring topographic highs, as proposed by Brüggen (1950), Hollingworth (1964) and Naranjo and Paskoff (1982), is supported by the following observations: (1) the linear features nearly completely encircle Cerro Soledad, on near horizontal levels (supplementary data, Fig. 3); (2) they are preserved in soft sedimentary rocks as well as in bedrock notches, which occur at exactly the same elevation (supplementary data, Fig. 3); (3) rounded pebbles occur localized at the bedrock notches and bedrock outcrops, and are absent elsewhere; (4) the pebbles are of the same lithology as the local bedrock, pebbles of allochthonous lithology are absent; (5) western, wind-exposed, flanks of the hills have wider platforms, as would be expected if wind fetch is important for their creation; (6) the Soledad formation is dominated by salar/lake deposits (Sáez et al., 1999; 2012; Quezada et al., 2013) and (7) bottom nucleated evaporites (supplement, Fig.2) record ephemeral open water conditions until the final stages of the deposition of the Soledad formation.

Alternative explanations for the platforms in sedimentary rocks, such as differential erosion due to variable degree and type of cementation and an absence of a lake, do not explain the repeated coincidence between the elevation of platforms in sedimentary rocks and bedrock notches and the near-horizontal nature of these linear features. However, it is possible that the creation or preservation of platform levels in sedimentary rocks is linked to enhanced cementation rather than wave action, since near-shore groundwater levels during lake stages would be identical to the corresponding lake levels. Explaining the occurrence of rounded pebbles by fluvial transport from elsewhere would be in conflict with the observation that allochthonous lithologies are absent and that pebble occurrences are limited to rare local bedrock outcrops.

The terraces along the (north-)western flanks of the Cerro Soledad are most easily recognized, both from satellite imagery (Fig. 3) and in the field. They are traceable throughout the hills protruding from the floor of the PDT (Fig. 3). Shorelines at the eastern, wind-averted flanks are less developed or absent. Shoreline formation due to wave-erosion was likely enhanced by the long wind fetch and a sufficiently deep water body upwind, as was available during lake-high stands of the QLSL (prevailing westerly winds had > 15 km fetch; see also Fig. 6). Wave action in lakes can erode shorelines that are tens of metres wide into bedrock within a few hundred years (Oviatt et al., 1992; Garcin et al., 2012; Lifton et al., 2015). While we do not know the strength of the paleo-winds and the kinetics of the shore erosion, we note that the setting of the ancient islands in the QLSL is conducive for shoreline formation. The pronounced aridity of the Atacama Desert, and the uplift of the shorelines above possible future lake-levels after their formation, aided their long-term preservation.

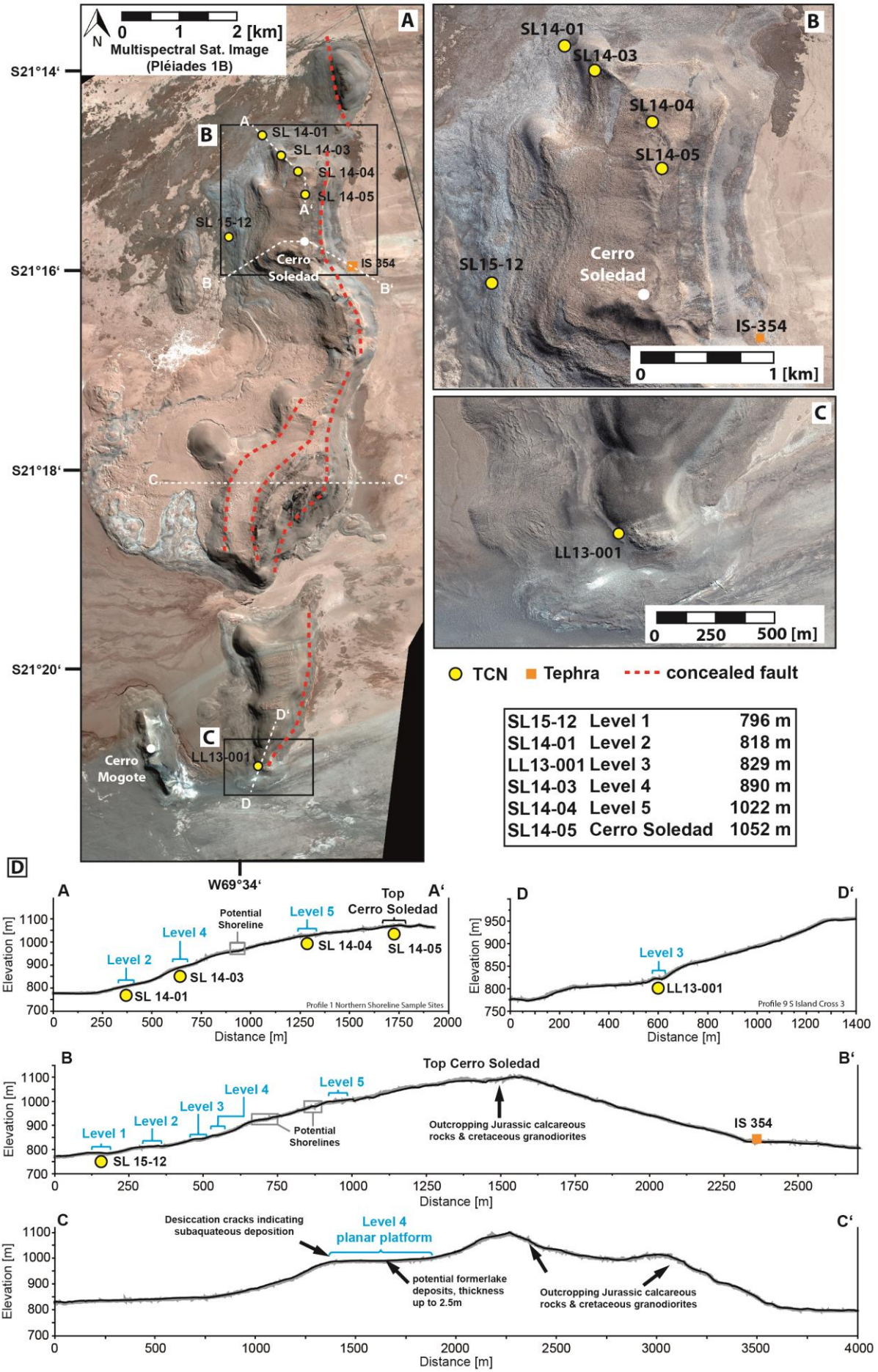
A
0 1 2 [km]
N
Multispectral Sat. Image
(Pléiades 1B)
S21°14'
S21°16'
S21°18'
S21°20'
B
SL 14-01
SL 14-03
SL 14-04
SL 14-05
SL 15-12
Cerro Soledad
IS 354
C
LL13-001
Cerro Mogote
W69°34'
B
SL14-01
SL14-03
SL14-04
SL14-05
SL15-12
Cerro Soledad
IS-354
0 1 [km]
C
LL13-001
0 250 500 [m]
TCN
Tephra
concealed fault
SL15-12 Level 1 796 m
SL14-01 Level 2 818 m
LL13-001 Level 3 829 m
SL14-03 Level 4 890 m
SL14-04 Level 5 1022 m
SL14-05 Cerro Soledad 1052 m
D
A
A'
Potential Shoreline
Top Cerro Soledad
Level 1
Level 2
Level 3
Level 4
Level 5
Elevation [m]
Distance [m]
Profile 1 Northern Shoreline Sample Sites
D
D'
Profile 9 S Island Cross 3
B
B'
Outcropping Jurassic calcareous rocks & cretaceous granodiorites
Potential Shorelines
C
C'
Desiccation cracks indicating subaqueous deposition
Level 4 planar platform
potential formerlake deposits, thickness up to 2.5m
Outcropping Jurassic calcareous rocks & cretaceous granodiorites

Fig. 3: (A-C) High resolution Pansharpened Multi-Spectral Image (Pléiades-1B) of the study area. Yellow dots indicate sampled shoreline terraces, orange square indicates dated tephra deposit (Quezada et al., 2013). White dashed lines highlight topographic profiles (D). Dashed red lines indicate potential concealed faults. (B) Northern island. (C) Southern island. (D) Topographic profiles based on a high resolution DEM (Pléiades-1B resolution ~60cm) of shorelines features. Corresponding and sampled shoreline terraces are marked, including potential shorelines terraces derived by DEM analysis. (Colour – Size: Full Page width 190mm)

Sampling locations

The bedrock of the paleo-islands, i.e. Jurassic marine sediments and volcanic rocks, at the northern island (Fig. 3A and 3B) joined by Cretaceous granodioritic rocks, is almost completely covered by evaporites of the Soledad Formation. Bedrock outcrops are limited to the tops of the paleo-islands (above ~1000 m elevation) and to spurs. Planar platforms are preserved in evaporitic cemented siliciclastic sediments and the bedrock spurs (Fig. 3A, D). Wave-cut platforms cut into the evaporites, however, are largely devoid of pebbles (and other rock clasts), whereas the wave-cut shorelines on bedrock have locally abundant pebbles. The variable abundance of pebbles suggests that they are locally derived, which is supported by the matching lithologies of pebbles and exposed bedrock.

We sampled small platforms on, or near spurs (LL13-001; SL-14-01; SL14-3; SL14-4; Fig. 3 A-C), below bedrock cliffs (LL13-001; SL-14-01; SL14-3), and on a planiform area near the summit of the northern island (SL14-05; Fig. 3 A-C). SL15-12 samples were retrieved from a wide platform at the western flank of the northern island. While it was cut into evaporitic-cemented siliciclastics, it harboured bedrock clasts and some pebbles. The bedrock fragments give this platform a different appearance in the field and on aerial photography (grey shades in Fig. 3; as compared to beige colours of the other evaporite platforms).

The height of the cliffs behind the bedrock platforms allows for a maximum of few meters of vertical erosion into the spurs (3-10 m), the amount of vertical erosion of rocks supplying the

293 pebbles on surfaces without a backing cliff is not constrained. Incomplete shielding/pre-exposure
294 can therefore be expected (Dunai, 2010). Since the shoreline deposits are thin (<50 cm thickness,
295 mostly <10 cm), depth profile sampling would not constrain pre-exposure of the sediments
296 (Dunai, 2010).

297 Site SL14-04 on the spur had no bedrock cliff. It was a shallow depression (ca. 10 cm lower than
298 surrounding bedrock; ca. 10 m^2 area) that had abundant, perfectly rounded pebbles, and only a
299 few fragmented clasts. This pebble deposit exhibits a weak patterning due to pelo- or
300 haloturbation (cryoturbation can be ruled out due to the prevailing climatic conditions).

301 Generally, post-depositional shielding of samples from cosmic rays due to intermittent burial, or
302 more likely in this case by exhumation of the samples originally deposited beneath a sedimentary
303 cover, cannot be excluded. The nature of the shoreline deposits renders it difficult ascertain if they
304 have eroded significantly since their deposition. The lack of extensive talus aprons downslope of
305 the shorelines, however, indicates that the shoreline deposits are predominantly well preserved.

306 At all sites our target materials were pebbles and bedrock clasts. The lithologies most amenable
307 for exposure dating (e.g. vein quartz and quartz-rich lithologies), tend to be less rounded than
308 quartz-poor/quartz-free lithologies; therefore, several clasts ($n \geq 6$) were sampled (only if
309 rounded pebbles were present at the same level). On finding localized concentrations of quartz
310 fragments, which may indicate *kernsprung* (splitting of pebbles), only one fragment per cluster
311 was sampled in order to avoid sampling multiple fragments of the same clast. In total we sampled
312 six sites, five on the northern island and one on the southern one (Fig. 3). The preserved rounding
313 of pebbles, and preserved angularity of clasts, allow for a few mm of erosion of the pebble surfaces
314 at most.

315 ## 3. Analytical methods

316 To determine single clast exposure ages we analysed quartz for ^{10}Be, ^{26}Al, and ^{21}Ne. The quartz
317 was prepared as AMS (Accelerator Mass Spectrometry) targets following either the standard

318 approach or the single-step column approach outlined in Binnie et al. (2015). The targets were
319 measured for ^{10}Be at CologneAMS (Dewald et al., 2013), normalized to the standards of Nishiizumi
320 et al. (2007). Neon isotope analyses were performed at SUERC following the procedures outlined
321 in Codilean et al. (2008) using the CREU quartz (Vermeesch et al., 2015) as internal standard.
322 Specific sample preparation and analysis details are in the supplementary data.

323 Exposure ages are derived from the CRONUS-Earth calculator version 2.0 (Marrero et al., 2016),
324 using the scaling factors of Lifton et al. (2015). Topographic shielding factors for each sample site
325 were measured in the field. We assumed a density of 2.65 g/cm^3, a zero erosion rate for the
326 pebbles and employed the 07KNSTD flag in the CRONUS-Earth calculator. Mean ages of
327 populations of clasts from one site were calculated after the removal of outliers, using Chauvenet's
328 Criterion (Taylor, 1997). Note, all age uncertainties reported are one standard deviation. Specific
329 details on the age calculation are in the supplementary data, including a geomagnetic database
330 sensitivity test using CREp (Martin et al., 2017). Analytical results and ages are provided in
331 Table 1.

332 ## 4. Results

333 The mean ^{10}Be exposure ages obtained for the shoreline deposits (Table 1; Fig. 4) span a wide
334 range: from ~275 ka at the lowest shoreline level (Level 1) to ~3 Ma for the deposits on the top
335 of the Cerro Soledad (Top). Several individual clasts have significantly older exposure ages than
336 the majority at a given site. Most probability density plots of exposure ages of the individual
337 locations (Fig. 4) have a positive skewness, with a tail towards higher ages. All outliers identified
338 by Chauvenet's Criterion (Taylor, 1997) are older ages. All ^{26}Al ages of individual clasts (n=5;
339 supplementary data) are concordant with the corresponding ^{10}Be ages. The combined ^{26}Al and
340 ^{10}Be data are consistent with a simple, single stage exposure history (see Supplementary data). In
341 one instance, site SL14-04, the scatter of the limited data did not permit the determination of a
342 meaningful average age (the limited number of measurements is due to the scarcity of quartz-
343 bearing clasts at that site). Individual ^{21}Ne exposure ages of clasts are either significantly higher

than the corresponding ^{10}Be ages of a specific site (shorelines SL14-01; SL14-03, SL14-04) or are concordant (e.g. SL14-05; top of Cerro Soledad).

In general, the cosmogenic nuclide data confound the expectation of significant pre-exposure for some clasts in each population, which is based on the limited mass removed for the creation of the shorelines. The first line of evidence for pre-exposure is the positive skewedness of ^{10}Be age-populations (Applegate et al., 2010); the second is the significantly higher ^{21}Ne-ages obtained in many samples (SL14-01, SL14-03, SL14-04), except for the highest shoreline (SL14-05). ^{21}Ne is stable, thus long-term production in partially shielded positions in the bedrock can add a higher pre-exposure signal than is possible for ^{10}Be, particularly if the duration of pre-exposure is protracted. In principle, the youngest age obtained would provide the most likely age, if periods of burial or exhumation have not occurred (Applegate et al., 2010). It appears that the process leading to the planation of the Top of Cerro Soledad removed sufficient material to obliterate a pre-exposure signal. Since we cannot exclude some exhumation (see previous section), the best estimations for the timing of shoreline formation are the arithmetic mean ^{10}Be ages, rather than the youngest ages obtained.

On top of Cerro Soledad (SL14-05, 1051 m) the mean ^{10}Be age is 2.92 ± 0.24 Ma (n=3). The corresponding ^{21}Ne age is indistinguishable from this (3.05 ± 0.12 Ma). All ^{10}Be and ^{21}Ne ages of individual clasts are concordant; indicating a continuous exposure for the clasts at the sampling location and negligible post-depositional exhumation. One clast at this sampling location has a significantly older age (4.5 ± 0.6 Ma ^{10}Be and 4.8 ± 0.2 Ma ^{21}Ne) and was not included in the mean (see Methods section). On shoreline level 5 (SL14-04, 1022 m) ^{10}Be ages vary between 260 ka and 4.5 Ma, while ^{21}Ne ages range from 1.9 Ma to 21.6 Ma. The ^{10}Be and ^{21}Ne ages of individual clasts are not concordant, with the ^{21}Ne ages being 3 to 4 times higher than the corresponding ^{10}Be ages. The highest ^{21}Ne exposure age (21.6±0.7 Ma) is amongst the oldest reported for the Atacama Desert (Dunai et al., 2005; Carrizo et al., 2008; Evenstar et al., 2009; Evenstar et al., 2017). Since a much longer exposure is unlikely, this indicates that the exhumation of the material that sourced the pebble was shallow. The high age dispersion is probably due to pre-exposure, combined with

371 pelo-/haloturbation inferred for this site (see section on sample locations), and prevents the
372 calculation of a meaningful age for this site. The mean ^{10}Be age from shoreline level 4 (SL14-03,
373 890 m) is 1.27 ± 0.47 Ma (n=5, all clasts). The mean ^{21}Ne age is significantly older at 1.85 ± 0.12
374 Ma (n=2). In one instance from this level, the ^{10}Be and ^{21}Ne ages of an individual clast agree.
375 Shoreline level 3 (LL13-001, 829 m) gives a mean ^{10}Be age of 540 ± 160 ka (n=5; one outlier). Due
376 to the generally small size of pebbles on this level no material for ^{21}Ne measurements could be
377 spared. On shoreline level 2 (SL14-01, 818 m) the mean ^{10}Be age is measured as 392 ± 37 ka (n=5;
378 one outlier). All ^{21}Ne ages of individual clasts are approximately twice the corresponding ^{10}Be
379 ages. The lowest elevation site, shoreline level 1 (SL15-12, 796 m), produces a mean ^{10}Be age of
380 274 ± 74 ka (n=5; one outlier). As with shoreline level 3, the paucity of quartz is such that no
381 material for ^{21}Ne measurements was available.

382 The mean ^{10}Be ages of shoreline levels shows a strong positive relationship with present day
383 elevation (Fig. 5), suggesting constant uplift. If shoreline levels were created at similar recurring
384 relative lake levels (relative to the paleo-island), the average tectonic uplift rate of the emergent
385 paleo-island is 94± 10 m/Ma (2σ). The present day elevations of the paleo-spillways are ~ 830 m
386 elevation and the Coastal Cordillera is uplifting relative to the Central Depression. Assuming
387 abandonment of the lowest preserved shoreline (level 5, 796m) because the spilling level at the
388 Río Loa canyon was breached (Fig. 2), the uplift rate of the Coastal Cordillera relative to this
389 shoreline is 160± 80 m/Ma. Utilizing the elevation-shoreline relationship (Fig. 5), we tentatively
390 assign an age of 2.5–2.8 Ma for the highest shoreline-level (SL04-4, 1022 m).

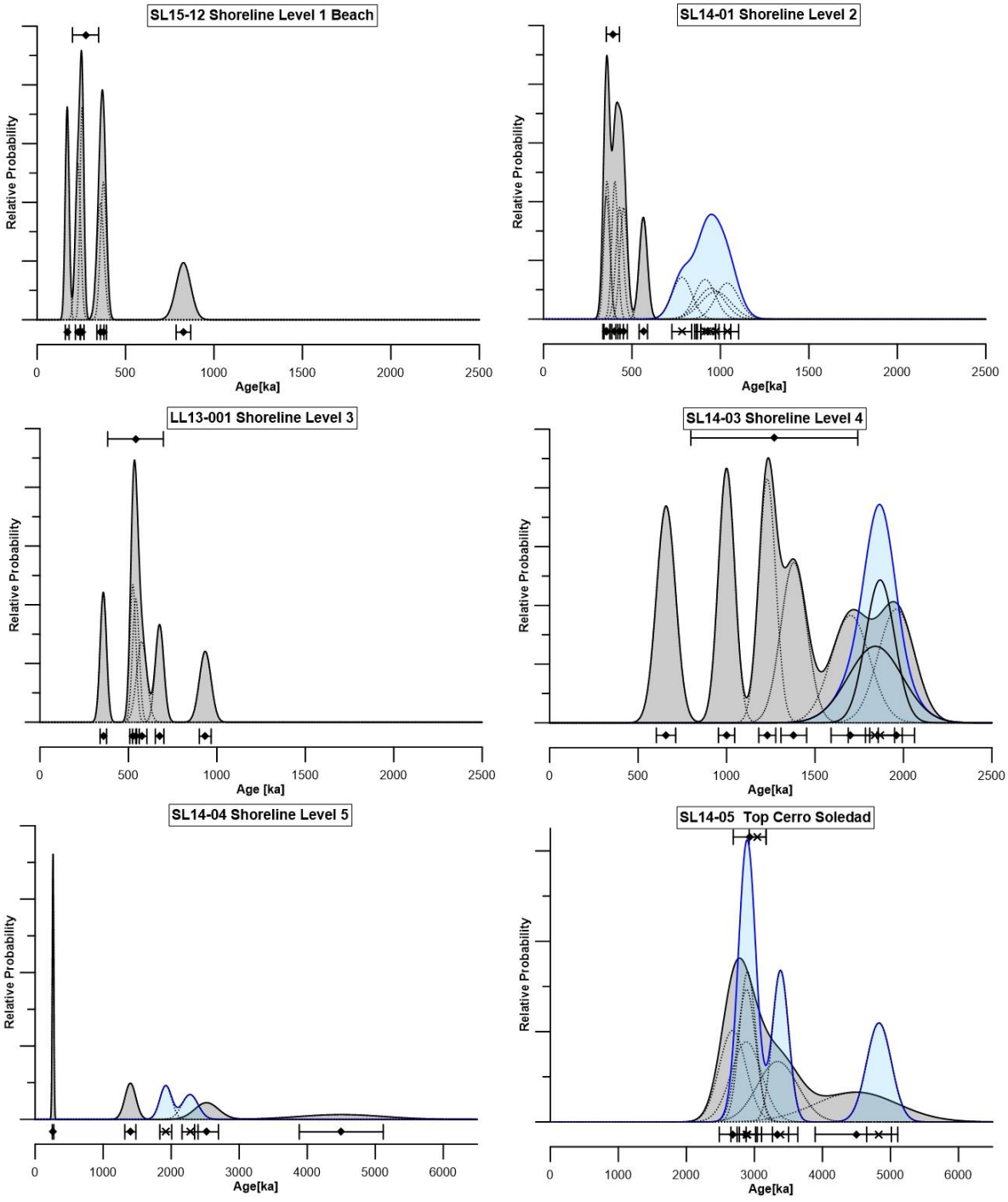

391

392 Fig. 4: Cumulative probability density plots of single clasts ^{10}Be (grey shading) and ^{21}Ne (blue
393 shading). Exposure ages for ^{10}Be are plotted as diamonds and ^{21}Ne as crosses underneath the
394 probability density plots. Error bars in this case are the 1 s.d. 'internal' age uncertainties (i.e.
395 analytical uncertainty only). Above the shaded probability envelopes are the relevant arithmetic
396 mean ages of shoreline terraces and hilltop deposits with one standard deviation error bars (see
397 supplementary data). *(Colour – Size: Full Page width 190mm)*

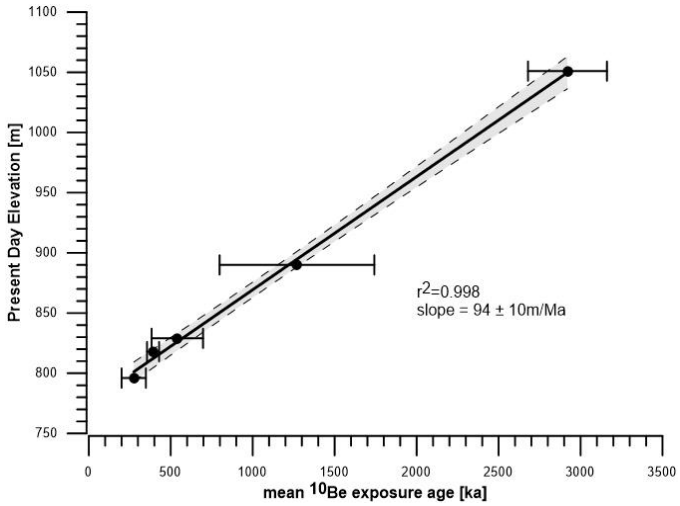

Fig. 5: Elevation versus mean ^{10}Be exposure ages for the five sample locations. Stippled lines represent the 95% confidence interval of the linear regression. Note the uncertainty on the slope (estimated uplift rate) is here ± 2σ. *(No-Colour – Size: Small column size 90mm)*

5. Discussion

The results indicate that at least five ephemeral lake phases occurred in the southern Central Depression between the late Pliocene (3.2-2.7 Ma, Top of Cerro Soledad) until the mid-Pleistocene (350-200 ka). These phases lasted sufficiently long to cut shorelines into bedrock and pre-existing/coeval evaporites of the Soledad Formation. We take the lack of intermediate shorelines between the highest (1022 m; tentative age 2.5–2.8 Ma) and the next youngest (890 m; 1.27 ± 0.47 Ma) as indication that no lake existed for a significant period of time between 2.65 ± 0.15 Ma and 1.27 ± 0.47 Ma. While elevation differences clearly separate the four youngest shorelines (1.27 ± 0.47 Ma at 890 m; 540 ± 160 ka at 829 m; 392 ± 37 ka at 818 m; 274 ± 74 ka at 796 m), the age resolution is insufficient to separate these lake phases. It is clear from the existence of paleo shorelines, however, that between 1.27 ± 0.47 Ma and 274 ± 74 ka at least four distinct lake phases occurred. The age of the youngest and lowest shoreline (274 ± 74 ka) records the onset of the incision of the present day Río Loa Canyon (Fig. 6); the incision transformed the Río Loa catchment into an exoreic catchment and marks the cessation of lacustrine sedimentation in the QLB. This interpretation for the onset of incision is based on the assumption that shoreline

418 terraces are only created during stable lake levels, which have to be of a sufficiently long duration
419 to allow enough wind-induced wave erosion. Moreover, based on the susceptibility of basin
420 sediments to erosion, we assume that the initial onset of incision happened fast as the sediments
421 were removed and decelerated once resistant bedrock was encountered. Prior to the incision, the
422 existence or absence of paleo-lakes mirrored the hydrological balance in the Río Loa catchment.

423 In the endoreic phase, i.e. prior to 274 ± 74 ka, the water balance in the lower Río Loa catchment
424 was likely to have been governed by precipitation sources in the Precordillera (above ~2500 m;
425 Houston and Hartley, 2003; Jordan et al., 2014) while evaporation (Houston, 2006a) and
426 groundwater discharge towards the coast (e.g. towards the Salar Grande; Chong et al., 1999;
427 Jordan et al., 2015a) provided the sinks. To balance present levels of evaporation (Houston,
428 2006a), the supply of water from Río Loa channel flow and groundwater must have been about
429 thirty times the modern discharge of the Río Loa at the coast (3.6 m^3/s; Salazar, 2003), in order to
430 form a lake of the dimension inferred for the QLSL (Fig. 6).

431 Assuming that evaporation in the Central Depression and groundwater discharge potential are
432 less variable than changes in precipitation, the paleo lake levels mostly represent changes in
433 precipitation in the catchment, i.e. they indicate wetter climatic conditions in the source areas of
434 the Precordillera. We therefore conclude that between 2.65 ± 0.15 Ma and 1.27 ± 0.47 Ma the
435 source area in the Precordillera was predominantly (hyper-)arid. After 1.27 ± 0.47 Ma the climate
436 in the source region had brief wetter interludes that were none-the-less long enough to erode
437 shorelines. Due to the current orders of magnitude difference in precipitation between the Central
438 Depression and the Precordillera (Houston and Hartley, 2003; Jordan et al., 2014) changes in the
439 paleo-lake reflect the paleoclimate of the distant source (Precordillera) more strongly than the
440 local (Central Depression) paleoclimate (Jordan et al., 2014). It is likely that the Central
441 Depression (< 1500 m) remained (hyper-)arid throughout the wetter phases indicated for the
442 Precordillera (Gayo et al., 2012; Jordan et al., 2014).

443 Two recent studies (Jordan et al., 2014; Wang et al., 2015) provide constraints on Plio-Pleistocene
444 changes in climate within the Río Loa catchment. A soil profile in the Central Depression in the

445 southernmost portion of the Río Loa catchment allowed Wang et al. (2015) to conclude that
446 climatic conditions were wetter than present between 3.2 and 2.5 Ma, and between 1.3–0.6 Ma.
447 Investigating soils and sediments of alluvial fan systems on the precordilleran foreslope, due east
448 of our study area, Jordan et al. (2014) infer wetter conditions for the periods between 4 and 3.6,
449 as well as between 2.6 and 2.2 Ma, but hyperarid conditions between 2.2 and 1 Ma. For the time
450 since ~1 Ma the authors infer hyperarid conditions with century to millennial scale fluctuations
451 to an arid climate in the alluvial fans source areas (Jordan et al., 2014). Our findings agree with
452 previous evidence for the cessation of a 'pluvial' phase at ~3 Ma and a later phase of pluvial
453 conditions around 1Ma in the Central Depression (Hartley, 2003; Placzek et al., 2010; Evenstar et
454 al., 2017). These brief, centennial to millennial interludes of wetter climate in the last 1 Ma (Jordan
455 et al., 2014) are sufficiently long to cut shorelines (Oviatt et al., 1992; Garcin et al., 2012; Lifton et
456 al., 2015). South of the Río Loa catchment, Jungers et al. (2013) suggested that enhanced erosion
457 and deposition between 250 and 400 ka are indicative of wetter conditions. We note that, despite
458 the considerable uncertainties of the ages and the different nature of the proxies, the inferred
459 pluvial periods (Jungers et al., 2013; Jordan et al., 2014; Wang et al., 2015) agree favourably with
460 our shoreline ages. The age-constraints from these studies (this study, Jungers et al., 2013; Jordan
461 et al., 2014; Wang et al., 2015), however, are not sufficiently precise to be able to associate them
462 to particular stadials/interstadials.

463 The Plio-Pleistocene sediments of the QLSL provide important paleoclimatological information
464 (Chong et al., 1999; Sáez et al., 1999; Pueyo et al., 2001; Sáez et al., 2012; Quezada et al., 2013).
465 The currently available chronological constraints (Sáez et al., 2012; Quezada et al., 2013; Jordan
466 et al., 2014, this study) are, however, contradictory. On Cerro Soledad (Fig. 1,3), the Soledad
467 evaporites directly overlay the intrusive substrate, lacking older Cenozoic sediments (Pueyo et al.,
468 2001). They cover the entire Cerro Soledad, bar the highest ridges (Pueyo et al., 2001; this study).
469 Interbedded volcanic ash layers in these evaporites yield Ar/Ar ages of 3.16 ± 0.07 Ma and
470 3.73 ± 0.02Ma (Quezada et al., 2013), indicating the temporal hiatus between the deposition of the
471 Soledad formation and the preceding Quillagua formation (termination ~4.5 Ma, Sáez et al., 2012)

was less than 750 ka, if indeed there was a hiatus. Near the eastern fringe of the QLSL, the Lomas del Sal (Fig. 1,6) is a tectonically uplifted block of the Soledad formation, with massive displacive halite ~90 m thick topped with ~10 m of gypsum cover (Pueyo et al., 2001). The halite is devoid of fluvioclastic sediments (Pueyo et al., 2001), whereas the gypsum cover contains interfingering alluvium (Jordan et al., 2014). Volcanic ashes found in a canyon near the bottom of the massive halite yield Ar/Ar ages between 0.21 ± 0.07 Ma and 0.098 ± 0.042Ma (Sáez et al., 2012); consequently, Sáez et al. (2012) place the Soledad Formation in its entirety into the mid to late Pleistocene. Based on the sedimentary horizons underlying the geomorphic surfaces, Jordan et al. (2014) assigned a Pliocene age (i.e. >2.6 Ma) for the evaporites at the top of the Lomas del Sal (Fig. 4 in Jordan et al., 2014). The latter clearly contradicts the findings of Sáez et al. (2012), however, it is in agreement with the ages of Quezada et al. (2013). While we cannot resolve the reasons for these contradictory results here, we note that our findings are rather in line with those of Jordan et al. (2014) and Quezada et al. (2013), since we present evidence for lake phases that eroded Soledad evaporites since the late Pliocene.

The endohereic drainage system of the QLB (Sáez et al., 1999), had three main lake phases (Hilaricos Fm, Quillagua Fm, Soledad Fm, Sáez et al. (1999)). The evolution of an endohereic drainage system in the QLB was initiated by differential uplift of the Coastal Cordillera in relation to the Central Depression. At the same time, localized subsidence of the Central Depression created further accommodation space (Jordan et al., 2015b; Cosentino and Jordan, 2017). The inferred spilling point of the last lake phase is located at a transpressional topographic high associated with the strike slip fault of the AFS. Lake deposits (diatomites and open water evaporites; supplementary data) are found exclusively to the east of this high point (Fig. 1). The topographic high is made up from older, presumably early Miocene, coarse-grained fluvioclastic sediments (age-equivalents of the Azapa and/or El Diablo formation; Evenstar et al., 2017). These sediments are unconsolidated, thus prone to fast fluvial erosion once spilling occurred. The first phase of canyon down cutting and drainage of the lake was, therefore, probably very fast. Once the drainage hit bedrock, currently 150-200 m above the present valley floor, incision might have

been slower. We cannot exclude that spilling of the lake occurred via headward erosion of drainage from groundwater sapping (Hoke et al., 2004; May et al., 2005), since ground water conductivity is high in unconsolidated coarse grained sediments. From the preservation of open water evaporites at the same elevation (±10m relative) as the inferred spilling point (supplementary data) we infer that the lake spilled, though sapping by shallow groundwater might have accelerated the process. The change from an endohereic to an exohereic drainage system terminated the existence of lakes in the QLB, triggering subsequent incision and widespread denudation of its lacustrine deposits.

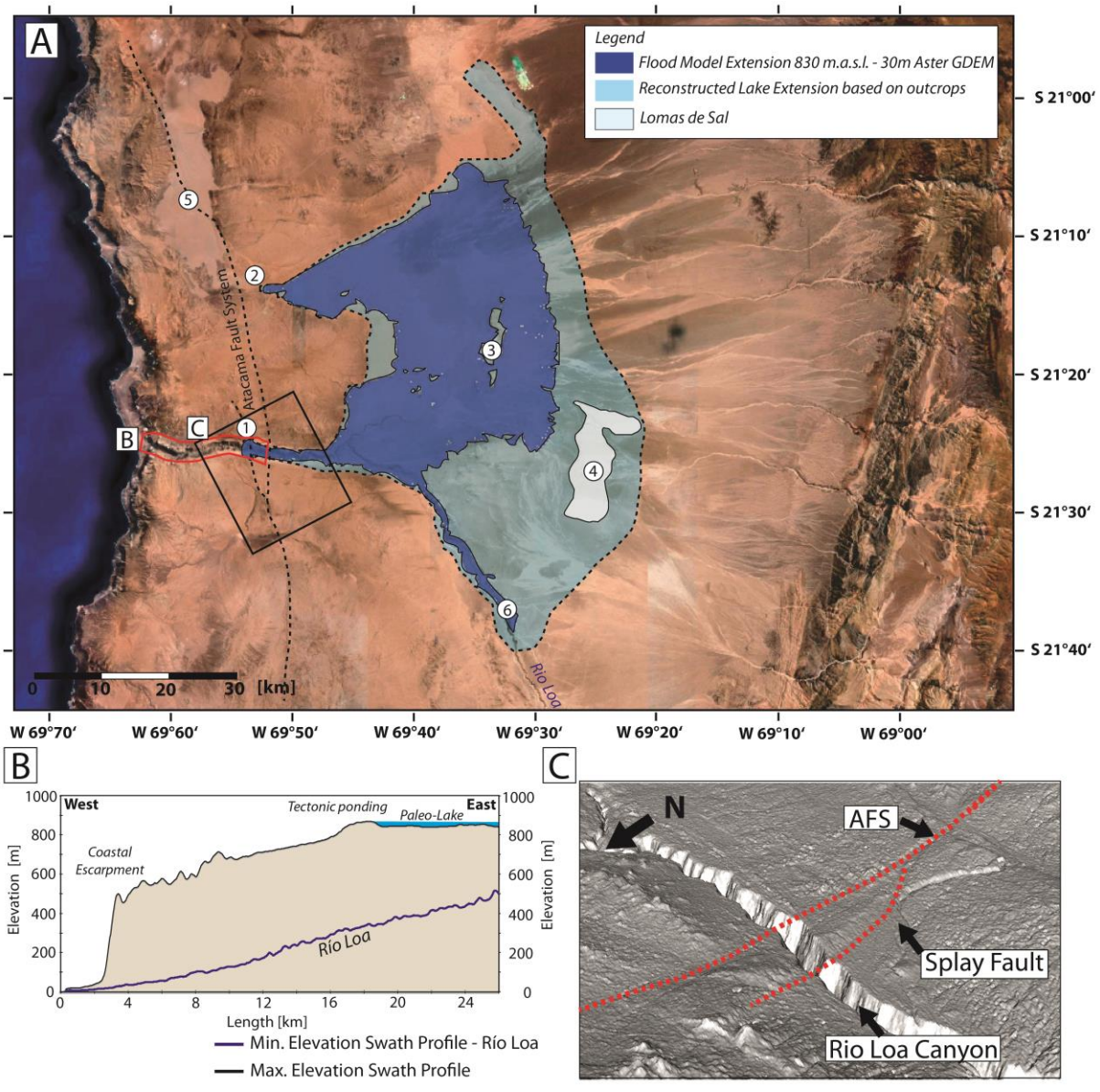

Fig. 6: Google Earth image with modelled lake extension (ASTER GDEM 30m resolution) of a flooding level (dark blue) of 830 m.a.s.l. (Rivertools 3.0). Reconstruction only for the Quillagua-Llamara basin. Light blue indicates reconstructed estimated maximum paleo- lake extension based on outcrops and modelled lake extensions (Rivertools 3.0). (1) Río Loa potential overflow divide towards the Pacific, (2) Montón de Gloria pass, overflow divide towards Salar Grande, (3) Cerro Soledad with isolated topographic heights, (4) Lomas de Sal, (5) Salar Grande, and (6) Quillagua. (B). Maximum elevation indicates local tectonic uplift of a splay fault from the AFS responsible for potential tectonic ponding. Minimum elevation indicates recent Río Loa course. (C) 3D Image (ASTER GDEM data) displays the tectonic splay fault from the Atacama Fault System. *(Colour – Size: Full Page width 190mm)*

6. Conclusion

The exposure age dating undertaken here better constrains the timing of pluvial periods in the Atacama Desert and the age for deposition of the Soledad Formation throughout the late Pliocene and Pleistocene. Shoreline formation and rounded pebbles on isolated topographic highs indicate tectonic activity throughout the Pleistocene and their uplift at rates of 94 m/Ma. Our results place the timing of the deposition of the Soledad Fm in the late Pliocene and Pleistocene under a wetter climate than today. Exposure ages of the youngest shoreline (274 ± 74 ka) constrain the timing for the incision of the modern Río Loa through the Coastal Cordillera and the transformation of the Río Loa catchment from an endohereic to exohereic system. Despite the Central Depression of the Atacama Desert remaining hyperarid through the Quaternary, climate changes external to the region can still have significant environmental impacts.

Acknowledgments

Thanks go to Luigia Di Nicola from SUERC for assisting during noble gas analysis. Furthermore, for help processing ^{10}Be and ^{26}Al data at the University of Cologne we thank Elena Voronina,

Damián López, and Tomasz Góral. We are grateful to Shasta Marrero for calculating ^{21}Ne ages with the new CRONUS Calculator MatLab version 2.0. We would like to thank Eduardo Campos and colleagues at the Universidad Catolica del Norte at Antofagasta for logistical support. Reviews by one anonymous reviewer, Teresa Jordan and Pierre-Henri Blard significantly improved the manuscript. This study was funded by the University of Cologne.

7. Appendices: Supplementary Material

Shoreline Level 1	Elevation [m.a.s.l.]	cosm. ^{21}Ne [10^7atoms/g]	cosm. ^{10}Be [10^6 atoms/g]	^{10}Be Age [kyr]	^{10}Be int. Uncert.[kyr]	^{10}Be Total Uncert. [kyr]	^{21}Ne Age [kyr]	^{21}Ne int. Uncert.[kyr]	^{21}Ne Total Uncert. [kyr]
SL 15-012 a	796	----------	3.42 ± 0.14	827	41	86			
SL 15-012 b	796	----------	1.12 ± 0.06	231	15	28			
SL 15-012 c	796	----------	0.82 ± 0.04	170	11	19			
SL 15-012 d	796	----------	1.66 ± 0.07	358	20	45			
SL 15-012 e	796	----------	1.21 ± 0.05	254	11	27			
SL 15-012 f	796	----------	1.71 ± 0.06	375	17	44			
Mean SL15-12			1.65 ± 0.07	360	253	260			
Mean Subpop. SL15-12 (b-f)			1.30 ± 0.34	274	74	77			
Shoreline Level 2									
SL 14-01 a	818	1.98 ± 0.18	1.94 ± 0.07	430	21	52	946	76	128
SL 14-01 b	818	2.03 ± 0.20	1.82 ± 0.07	403	17	39	974	85	144
SL 14-01 c	818	1.55 ± 0.18	1.63 ± 0.06	355	19	43	782	56	82
SL 14-01 d	818	2.18 ± 0.13	2.00 ± 0.08	453	21	49	1038	65	146
SL 14-01 e	818	1.87 ± 0.16	1.64 ± 0.06	359	17	44	913	59	106
SL14-01 f	818	----------	2.41 ± 0.84	564	23	56	928	64	105
Mean SL14-01			1.91 ± 0.07	417	74	84	953	72	128
Mean Subpop. SL14-01 (a-e)			1.80 ± 0.07	392	37	52			
Shoreline Level 3									
LL13-001 a	829	----------	3.89 ± 0.13	934	33	83			
LL13-001 b	829	----------	2.33 ± 0.08	525	17	48			
LL13-001 c	829	----------	1.68 ± 0.06	358	18	44			
LL13-001 d	829	----------	2.41 ± 0.08	542	19	49			
LL13-001 e	829	----------	2.54 ± 0.11	575	29	65			
LL13-001 f	829	----------	2.86 ± 0.09	676	24	77			
Mean Subpop. LL13-001 (b, c, d,e,f)			2.53 ± 0.09	540	160	160			
Shoreline Level 4									
SL14-03 a	890	4.02 ± 0.30	4.77 ± 0.17	1230	50	110	1840	150	270
SL14-03 b	890	4.07 ± 0.18	6.02 ± 0.21	1700	110	260	1870	80	270
SL14-03 c	890	----------	6.53 ± 0.23	1960	100	250			
SL14-03 d	890	----------	4.02 ± 0.15	1000	50	100			
SL14-03 f	890	----------	2.76 ± 0.15	658	50	100			
SL14-03 g	890	----------	5.32 ± 0.20	1380	100	170			
Mean SL14-03			4.90 ± 1.26	1270	470	490	1850	120	280
Shoreline Level 5									
SL14-04 a	1022	5.50 ± 0.27	----------				2280	120	320
SL14-04 b	1022	43.13 ± 1.40	10.40 ± 0.35	4500	620	1500	21600		700
SL14-04 c	1022	4.61 ± 0.21	1.36 ± 0.06	263	10	27	1920	90	230
SL14-04 g	1022	----------	5.93 ± 0.23	1400	80	180			
SL14-04 h	1022	----------	8.29 ± 0.28	2520	180	460			
Top Cerro Soledad									
SL14-05 a	1051	6.99 ± 0.32	8.99 ± 0.30	2880	230	590	2880	140	390
SL14-05 b	1051	11.57 ± 0.43	10.50 ± 0.35	4500	610	1500	4830	180	640
SL14-05 c	1051	7.03 ± 0.28	8.71 ± 0.29	2680	200	520	2900	120	390
SL14-05 e	1051	8.10 ± 0.28	9.47 ± 0.31	3340	300	780	3380	120	450
Mean SL14-05			9.42 ± 0.31	3220	610	910	3490	140	470
Mean Subpop. SL14-05 (a,c,e)			9.06 ± 0.31	2930	240	610	3050	130	410

539

Table 1. Cosmogenic isotope data for quartz clasts. Further information concerning site specific data, triple isotope plots and scaled production rates are given in the supplementary information section.

References

Aceituno, P., 1988, On the functioning of the Southern Oscillation in the South American sector. Part I: Surface climate: Monthly Weather Review, v. 116, no. 3, p. 505-524.

Allmendinger, R. W., and Gonzalez, G., 2010, Invited review paper: Neogene to Quaternary tectonics of the coastal Cordillera, northern Chile: Tectonophysics, v. 495, no. 1-2, p. 93-110.

Allmendinger, R. W., Gonzalez, G., Yu, J., Hoke, G., and Isacks, B., 2005, Trench-parallel shortening in the Northern Chilean Forearc: Tectonic and climatic implications: Geological Society of America Bulletin, v. 117, no. 1-2, p. 89-104.

Applegate, P. J., Urban, N. M., Laabs, B. J. C., Keller, K., and Alley, R. B., 2010, Modeling the statistical distributions of cosmogenic exposure dates from moraines: Geoscientific Model Development, v. 3, no. 1, p. 293-307.

Betancourt, J. L., Latorre, C., Rech, J. A., Quade, J., and Rylander, K. A., 2000, A 22,000-year record of Monsoonal precipitation from Northern Chile's Atacama Desert: Science, v. 289, p. 1542-1546.

Binnie, S. A., Dunai, T. J., Voronina, E., Goral, T., Heinze, S., and Dewald, A., 2015, Separation of Be and Al for AMS using single-step column chromatography: Nuclear Instruments and Methods in Physics Research Section B: Beam Interactions with Materials and Atoms.

Bozkurt, D., Rondanelli, R., Garreaud, R., and Arriagada, A., 2016, Impact of Warmer Eastern Tropical Pacific SST on the March 2015 Atacama Floods: Monthly Weather Review, v. 144, no. 11, p. 4441-4460.

Brüggen, J., 1950, Fundamentos de la Gelogia de Chile: Inst. Geog. Milit (Chile) p. 374 pp.

Carrizo, D., Gonzalez, G., and Dunai, T., 2008, Neogene constriction in the northern Chilean Coastal Cordillera: Neotectonics and surface dating using cosmogenic 21Ne: Revista Geologica De Chile, v. 35, no. 1, p. 1-38.

Chong, G., Mendoza, M., García-Veigas, J., Pueyo, J. J., and Turner, P., 1999, Evolution and geochemical signatures in a Neogene forearc evaporitic basin: the Salar Grande (Central Andes of Chile): Palaeogeography, Palaeoclimatology, Palaeoecology, v. 151, no. 1, p. 39-54.

Codilean, A. T., Bishop, P., Stuart, F. M., Hoey, T. B., Fabel, D., and Freeman, S. P., 2008, Single-grain cosmogenic 21Ne concentrations in fluvial sediments reveal spatially variable erosion rates: Geology, v. 36, no. 2, p. 159-162.

Contreras, S., Lange, C. B., Pantoja, S., Lavik, G., Rincón-Martínez, D., and Kuypers, M. M., 2010, A rainy northern Atacama Desert during the last interglacial: Geophysical Research Letters, v. 37, no. 23.

Cosentino, N. J., and Jordan, T. E., 2017, 87Sr/86Sr of calcium sulfate in ancient soils of hyperarid settings as a paleoaltitude proxy: Pliocene to Quaternary constraints for northern Chile (19.5–21.7° S): Tectonics, v. 36, no. 1, p. 137-162.

Cristini, L., Grosfeld, K., Butzin, M., and Lohmann, G., 2012, Influence of the opening of the Drake Passage on the Cenozoic Antarctic Ice Sheet: a modeling approach: Palaeogeography, Palaeoclimatology, Palaeoecology, v. 339, p. 66-73.

Dewald, A., Heinze, S., Jolie, J., Zilges, A., Dunai, T., Rethemeyer, J., Melles, M., Staubwasser, M., Kuczewski, B., Richter, J., Radtke, U., von Blanckenburg, F., and Klein, M., 2013, CologneAMS, a dedicated center for accelerator mass spectrometry in Germany: Nuclear Instruments & Methods in Physics Research Section B-Beam Interactions with Materials and Atoms, v. 294, p. 18-23.

587 Dunai, T. J., 2010, Cosmogenic Nuclides: Principles, concepts and applications in the Earth surface
588 sciences, Cambridge University Press.
589 Dunai, T. J., González López, G. A., and Juez-Larré, J., 2005, Oligocene–Miocene age of aridity in the
590 Atacama Desert revealed by exposure dating of erosion-sensitive landforms: Geology, v. 33,
591 no. 4, p. 321.
592 Evenstar, L., Mather, A., Hartley, A., Stuart, F., Sparks, R., and Cooper, F., 2017, Geomorphology on
593 geologic timescales: Evolution of the late Cenozoic Pacific paleosurface in Northern Chile and
594 Southern Peru: Earth-Science Reviews.
595 Evenstar, L. A., Hartley, A. J., Stuart, F. M., Mather, A. E., Rice, C. M., and Chong, G., 2009, Multiphase
596 development of the Atacama Planation Surface recorded by cosmogenic 3He exposure ages:
597 Implications for uplift and Cenozoic climate change in western South America: Geology, v. 37,
598 no. 1, p. 27-30.
599 Garcin, Y., Melnick, D., Strecker, M. R., Olago, D., and Tiercelin, J.-J., 2012, East African mid-Holocene
600 wet–dry transition recorded in palaeo-shorelines of Lake Turkana, northern Kenya Rift: Earth
601 and Planetary Science Letters, v. 331, p. 322-334.
602 Garreaud, R. D., Molina, A., and Farias, M., 2010, Andean uplift, ocean cooling and Atacama
603 hyperaridity: A climate modeling perspective: Earth and Planetary Science Letters, v. 292, no.
604 1-2, p. 39-50.
605 Gaupp, R., Kott, A., and Worner, G., 1999, Palaeoclimatic implications of Mio-Pliocene sedimentation
606 in the high-altitude intra-arc Lauca Basin of northern Chile: Palaeogeography
607 Palaeoclimatology Palaeoecology, v. 151, no. 1-3, p. 79-100.
608 Gayo, E. M., Latorre, C., Jordan, T. E., Nester, P. L., Estay, S. A., Ojeda, K. F., and Santoro, C. M., 2012,
609 Late Quaternary hydrological and ecological changes in the hyperarid core of the northern
610 Atacama Desert (~21°S): Earth-Science Reviews, v. 113, no. 3-4, p. 120-140.
611 Hartley, A. J., 2003, Andean uplift and climate change: Journal Geol. Soc. Lond., v. 160, p. 7-10.
612 Hartley, A. J., and Chong, G., 2002, Late Pliocene age for the Atacama Desert: Implications for the
613 desertification of western South America: Geology, v. 30, p. 43-46.
614 Hartley, A. J., Chong, G., Houston, J., and Mather, A. E., 2005, 150 million years of climatic stability:
615 evidence from the Atacama Desert, northern Chile: J. Geol. Soc., v. 162, p. 421-424.
616 Hartley, A. J., and Evenstar, L., 2010, Cenozoic stratigraphic development in the north Chilean
617 forearc: Implications for basin development and uplift history of the Central Andean margin:
618 Tectonophysics, v. 495, no. 1-2, p. 67-77.
619 Hoke, G. D., Isacks, B. L., Jordan, T. E., and Jennifer, S. Y., 2004, Groundwater-sapping origin for the
620 giant quebradas of northern Chile: Geology, v. 32, no. 7, p. 605-608.
621 Hollingworth, S., 1964, Dating the uplift of the Andes of northern Chile: Nature, v. 201, p. 17-20.
622 Houston, J., 2006a, Evaporation in the Atacama Desert: An empirical study of spatio-temporal
623 variations and their causes: Journal of Hydrology, v. 330, no. 3-4, p. 402-412.
624 Houston, J., 2006b, The great Atacama flood of 2001 and its implications for Andean hydrology:
625 Hydrological Processes, v. 20, no. 3, p. 591-610.
626 Houston, J., 2006c, Variability of precipitation in the Atacama Desert: its causes and hydrological
627 impact: International Journal of Climatology, v. 26, no. 15, p. 2181-2198.
628 Houston, J., and Hartley, A. J., 2003, The Central Andean west-slope rainshadow and its potential
629 contribution to the origin of hyper-aridity in the Atacama desert: International Journal of
630 Climatology, v. 23, p. 1453-1464.
631 Jensen, A., Dörr, M., Gotze, H., Kiefer, E., Ibbeken, E., and Wilke, H., Subsidence and sedimentation of
632 a forearc-hosted, continental pull-apart basin: the Quillagua trough between 21 30 and 21 45
633 S, northern Chile, *in* Proceedings Recent and Ancient Lacustrine Systems in Convergent
634 Margins. GLOPALS-IAS Meeting, Antofagasta, Chile, Abstracts1995, p. 5-6.
635 Jordan, T., Lameli, C. H., Kirk-Lawlor, N., and Godfrey, L., 2015a, Architecture of the aquifers of the
636 Calama Basin, Loa catchment basin, northern Chile: Geosphere, p. GES01176. 01171.
637 Jordan, T. E., Cosentino, N. J., and Jensen, A., 2015b, Pliocene-Quaternary Tectonic Subsidence of
638 part of the Central Depression Forearc, 20-22°S: XIV Congreso Geológico Chileno (La Serena).

639 Jordan, T. E., Kirk-Lawlor, N. E., Blanco P., N., Rech, J. A., and Cosentino, N. J., 2014, Landscape
640 modification in response to repeated onset of hyperarid paleoclimate states since 14 Ma,
641 Atacama Desert, Chile: Geological Society of America Bulletin.
642 Jordan, T. E., Nester, P. L., Blanco, N., Hoke, G. D., Dávila, F., and Tomlinson, A. J., 2010, Uplift of the
643 Altiplano-Puna plateau: A view from the west: Tectonics, v. 29, no. 5, p. n/a-n/a.
644 Jungers, M. C., Heimsath, A. M., Amundson, R., Balco, G., Shuster, D., and Chong, G., 2013, Active
645 erosion–deposition cycles in the hyperarid Atacama Desert of Northern Chile: Earth and
646 Planetary Science Letters, v. 371-372, p. 125-133.
647 Kirk-Lawlor, N., Jordan, T. L., Rech, J. A., and Lehman, S. B., 2013, Late Miocene to Early Pliocene
648 paleohydrology and landscape evolution of Northern Chile, 19° to 20° S: Palaegeography
649 Palaeoclimatology Palaeoecology, v. 387, p. 76-90.
650 Kober, F., Ivy-Ochs, S., Schlunegger, F., Baur, H., Kubik, P. W., and Wieler, R., 2007, Denudation rates
651 and a topography-driven rainfall threshold in northern Chile: Multiple cosmogenic nuclide
652 data and sediment yield budgets: Geomorphology, v. 83, p. 97-120.
653 Latorre, C., Betancourt, J. L., and Arroyo, M. T. K., 2006, Late Quaternary vegetation and climate
654 history of a perennial river canyon in the Río Salado basin (22°S) of Northern Chile:
655 Quaternary Research, v. 65, no. 3, p. 450-466.
656 Lifton, N., Caffee, M., Finkel, R., Marrero, S., Nishiizumi, K., Phillips, F. M., Goehring, B., Gosse, J.,
657 Stone, J., Schaefer, J., Theriault, B., Jull, A. J. T., and Fifield, K., 2015, In situ cosmogenic
658 nuclide production rate calibration for the CRONUS-Earth project from Lake Bonneville, Utah,
659 shoreline features: Quaternary Geochronology, v. 26, p. 56-69.
660 Marrero, S. M., Phillips, F. M., Borchers, B., Lifton, N., Aumer, R., and Balco, G., 2016, Cosmogenic
661 nuclide systematics and the CRONUScalc program: Quaternary Geochronology, v. 31, p. 160-
662 187.
663 Martin, L., Blard, P.-H., Balco, G., Lavé, J., Delunel, R., Lifton, N., and Laurent, V., 2017, The CREp
664 program and the ICE-D production rate calibration database: A fully parameterizable and
665 updated online tool to compute cosmic-ray exposure ages: Quaternary geochronology, v. 38,
666 p. 25-49.
667 May, G., Hartley, A. J., Chong, G., Stuart, F., Turner, P., and Kape, S. J., 2005, Litoestratigrafía,
668 cronoestratigrafía durante el Eoceno al Pleistoceno y evolución tectono-sedimentaria de la
669 Cuenca de Calama, norte de Chile: Revista geológica de Chile, v. 32, no. 1, p. 33-58.
670 McKay, C. P., Friedmann, E. I., Gómez-Silva, B., Cáceres-Villanueva, L., Andersen, D. T., and Landheim,
671 R., 2003, Temperature and moisture conditions for life in the extreme arid region of the
672 Atacama Desert: four years of observations including the El Niño of 1997-1998: Astrobiology,
673 v. 3, no. 2, p. 393-406.
674 Naranjo, J. A., and Paskoff, R. P., 1982, Estratigrafı´a de las unidades sedimentarias cenozoicas de la
675 Cuenca del Rı´o Loa en la Pampa del Tamarugal, Regio´n de Antofagasta, Chile: Rev. Geol.
676 Chile 15, v. 49-57.
677 Nester, P., 2008, Basin and paleoclimate evolution of the Pampa del Tamarugal forearc valley,
678 Atacama Desert, northern Chile: Cornell Theses and Dissertations, v.
679 http://hdl.handle.net/1813/10484.
680 Nester, P., and Jordan, T., 2012, The Pampa del Tamarugal Forearc Basin in Northern Chile: The
681 Interaction of Tectonics and Climate, Tectonics of Sedimentary Basins, John Wiley & Sons,
682 Ltd, p. 369-381.
683 Nester, P. L., Gayo, E., Latorre, C., Jordan, T. E., and Blanco, N., 2007, Perennial stream discharge in
684 the hyperarid Atacama Desert of northern Chile during the latest Pleistocene: Proceedings of
685 the National Academy of Sciences of the United States of America, v. 104, no. 50, p. 19724-
686 19729.
687 Nishiizumi, K., Caffee, M. W., Finkel, R. C., Brimhall, G., and Mote, G., 2005, Remnants of a fossil
688 alluvial fan landscape of Miocene age in the Atacama desert of northern Chile using
689 cosmogenic nuclide exposure age dating: Earth Planet. Sci. Lett., v. 237, p. 499-507.

690 Nishiizumi, K., Imamura, M., Caffee, M. W., Southon, J. R., Finkel, R. C., and McAninch, J., 2007,
691 Absolute calibration of Be-10 AMS standards: Nucl. Instr. Meth. Phys. Res. B, v. 258, p. 403-
692 413.
693 Ortlieb, L., Diaz, A., and Guzman, N., 1996, A warm interglacial episode during Oxygen Isotope Stage
694 11 in northern Chile: Quaternary Science Reviews, v. 15, no. 8, p. 857-871.
695 Oviatt, C. G., Currey, D. R., and Sack, D., 1992, Radiocarbon chronology of Lake Bonneville, eastern
696 Great Basin, USA: Palaeogeography, Palaeoclimatology, Palaeoecology, v. 99, no. 3-4, p. 225-
697 241.
698 Placzek, C. J., Matmon, A., Granger, D. E., Quade, J., and Niedermann, S., 2010, Evidence for active
699 landscape evolution in the hyperarid Atacama from multiple terrestrial cosmogenic nuclides:
700 Earth and Planetary Science Letters, v. 295, no. 1-2, p. 12-20.
701 Pueyo, J. J., Chong, G., and Jensen, A., 2001, Neogene evaporites in desert volcanic environments:
702 Atacama Desert, northern Chile: Sedimentology, v. 48, no. 6, p. 1411-1431.
703 Quezada, A., Vásquez, P., and Sepúlveda, F., 2013, Soledad Formation: mapping and radiometric
704 ages, Atacama Desert, I Region, Chile: GEOSUR.
705 Quezada, A., Vasquez, P., Sepúlveda, F., Blanco, N., and Tomlinson, A. J., 2012, Mapa Compilación
706 Geológica Área Quillagua - Salar Grande 1:100.000: Servicio Nacional de Geologica y Mineria
707 Gobierno Regional de Tarapacá.
708 Rech, J. A., Currie, B. S., Michalski, G., and Cowan, A. M., 2006, Neogene climate change and uplift in
709 the Atacama Desert, Chile: Geology, v. 34, no. 9, p. 761-764.
710 Rech, J. A., Currie, B. S., Shullenberger, E. D., Dunagan, S. P., Jordan, T. E., Blanco, N., Tomlinson, A. J.,
711 Rowe, H. D., and Houston, J., 2010, Evidence for the development of the Andean rain shadow
712 from a Neogene isotopic record in the Atacama Desert, Chile: Earth and Planetary Science
713 Letters, v. 292, no. 3-4, p. 371-382.
714 Rech, J. A., Quade, J., and Hart, W. S., 2003, Isotopic evidence for the source of Ca and S in soil
715 gypsum, anhydrite and calcite in the Atacama Desert, Chile: Geochim. Cosmochim. Acta, v.
716 67, p. 575-586.
717 Rieu, M., 1975, Les formations sedimentaires de la Pampa del Tamarugal et le rı´o Loa (Norte Grande
718 du Chili). : Fr. Off. Rech. Sci. Tech. Outre-Mer, Cah., Ser. Geol. 7 (2), 145–164.
719 Sáez, A., Cabrera, L., Garcés, M., Bogaard, P. v. d., Jensen, A., and Gimeno, D., 2012, The stratigraphic
720 record of changing hyperaridity in the Atacama desert over the last 10Ma: Earth and
721 Planetary Science Letters, v. 355-356, p. 32-38.
722 Sáez, A., Cabrera, L., Jensen, A., and Chong, G., 1999, Late Neogene lacustrine record and
723 palaeogeography in the Quillagua–Llamara basin, Central Andean fore-arc (northern Chile):
724 Palaeogeography, Palaeoclimatology, Palaeoecology, v. 151, no. 1, p. 5-37.
725 Salazar, C., 2003, Situación de los recursos hídricos en Chile, Situación de los recursos hídricos en
726 Chile, Centro del Tercer Mundo para el Manejo del Agua, A. C.
727 Sillitoe, R. H., and McKee, E. H., 1996, Age of supergene oxidation and enrichment in the Chilean
728 porphyry copper province: Economic Geology, v. 91, no. 1, p. 164-179.
729 Stoertz, G. E., and Ericksen, G. E., 1974, Geology of salars in northern Chile: U.S. Geol. Surv. Prof. Pap.
730 811, p. 65 pp.
731 Taylor, J., 1997, Introduction to error analysis, the study of uncertainties in physical measurements.
732 Vermeesch, P., Balco, G., Blard, P. H., Dunai, T. J., Kober, F., Niedermann, S., Shuster, D. L., Strasky, S.,
733 Stuart, F. M., Wieler, R., and Zimmermann, L., 2015, Interlaboratory comparison of
734 cosmogenic Ne-21 in quartz: Quaternary Geochronology, v. 26, p. 20-28.
735 Victor, P., Oncken, O., and Glodny, J., 2004, Uplift of the western Altiplano plateau: Evidence from
736 the Precordillera between 20° and 21°S (northern Chile): Tectonics, v. 23, no. 4, p. n/a-n/a.
737 Vuille, M., 1999, Atmospheric circulation over the Bolivian Altiplano during dry and wet periods and
738 extreme phases of the Southern Oscillation: International Journal of Climatology, v. 19, no.
739 14, p. 1579-1600.
740 Vuille, M., and Ammann, C., 1997, Regional snowfall patterns in the high, arid Andes, Climatic Change
741 at High Elevation Sites, Springer, p. 181-191.

Vuille, M., Bradley, R. S., and Keimig, F., 2000, Interannual climate variability in the Central Andes and its relation to tropical Pacific and Atlantic forcing: Journal of Geophysical Research-Atmostpheres, v. 105, no. D10, p. 12447-12460.

Vuille, M., and Keimig, F., 2004, Interannual variability of summertime convective cloudiness and precipitation in the central Andes derived from ISCCP-B3 data: Journal of Climate, v. 17, no. 17, p. 3334-3348.

Wang, F., Michalski, G., Seo, J.-H., Granger, D. E., Lifton, N., and Caffee, M., 2015, Beryllium-10 concentrations in the hyper-arid soils in the Atacama Desert, Chile: Implications for arid soil formation rates and El Niño driven changes in Pliocene precipitation: Geochimica et Cosmochimica Acta, v. 160, p. 227-242.

Wilcox, A. C., Escauriaza, C., Agredano, R., Mignot, E., Zuazo, V., Otárola, S., Castro, L., Gironás, J., Cienfuegos, R., and Mao, L., 2016, An integrated analysis of the March 2015 Atacama floods: Geophysical Research Letters, v. 43, no. 15, p. 8035-8043.

Woodman, R. F., 1998, Los lagos de Sechura: Informe Interno del Instituto Geofísico del Perú.

Zachos, J., Pagani, M., Sloan, L., Thomas, E., and Billups, K., 2001, Trends, rhythms, and aberrations in global climate 65 Ma to present: Science, v. 292, no. 5517, p. 686-693.